

SCIENTIFIC REPORTS

OPEN

Effect of Polarization Coulomb Field Scattering on Electrical Properties of the 70-nm Gate-Length AlGaIn/GaN HEMTs

Peng Cui¹, Yuanjie Lv², Chen Fu¹, Huan Liu³, Aijie Cheng³, Chongbiao Luan⁴, Yang Zhou⁵ & Zhaojun Lin¹

This research presents the first experimental observation of the enhancement of the polarization Coulomb field (PCF) scattering by aggressive lateral scaling of GaN HEMTs. By decreasing the source-drain distance to 300 nm through n^+ -GaN ohmic regrowth, 70-nm gate AlGaIn/GaN HEMTs achieved an extremely low electron mobility. Different from the electron mobility of the traditional device, which was determined by polar optical phonon scattering, the electron mobility of the 70-nm gate AlGaIn/GaN HEMTs was dominated by PCF scattering due to the enhanced nonuniform strain distribution of the AlGaIn barrier layer. Furthermore, compared with the parasitic access resistance at gate-source voltage $V_{GS} = 0V$, the parasitic access resistance at $V_{GS} = -2.5V$ showed an increase of approximately 700%, which was also responsible for the enhanced PCF scattering.

AlGaIn/GaN high electron mobility transistors (HEMTs) have shown excellent performance in the RF domain due to their high electron velocities and large sheet electron densities^{1–6}. In RF applications, the cutoff frequency (f_T), maximum oscillation frequency (f_{max}), and maximum drain current are the key device performance parameters^{1,7–9}. Many innovative device scaling technologies have been presented^{10–16}, and device scaling successfully increases the f_T and f_{max} of GaN HEMTs^{17–20}. However, because of the piezoelectric and spontaneous polarization, there are polarization charges at the AlGaIn/GaN interface^{21–24}. Under the gate bias, the polarization charges of the AlGaIn barrier layer under the gate region change due to the converse piezoelectric effect, which causes the strain distribution of the AlGaIn barrier layer to be altered^{25–27}. The strain distribution variation is more obvious with device scaling; as a result, the strain-distribution-dependent polarization Coulomb field scattering has a stronger influence on the electron transport^{28–35}, and the RF application of AlGaIn/GaN HEMTs is affected. Therefore, it is essential to investigate this influence to further improve the RF device performance of AlGaIn/GaN HEMTs.

In this research, 70-nm gate AlGaIn/GaN HEMTs with different source-drain distances ($L_{SD} = 300/600$ nm) and gate widths ($W_G = 20/40$ μm) were fabricated. Based on the measured current-voltage characteristics and the obtained two-dimensional electron gas (2DEG) electron densities, the electron mobility and parasitic access resistances were determined, and the influence of the strain distribution on the 70-nm gate AlGaIn/GaN HEMTs was explored.

Results and Discussion

The schematic of the AlGaIn/GaN HEMTs were shown in Fig. 1(a). As shown in Fig. 1(b), the device with $L_{SD} = 300$ nm and $W_G = 20$ μm was labeled as Sample 1, the device with $L_{SD} = 600$ nm and $W_G = 20$ μm as Sample 2, the device with $L_{SD} = 600$ nm and $W_G = 40$ μm as Sample 3. The I – V output characteristics and transfer characteristics (at drain-source voltage $V_{DS} = 4$ V) of the three samples were measured, as shown in Fig. 2. For decreasing the influence of the short-channel effect, the values of the measured drain-source current I_{DS} with a drain-source

¹School of Microelectronics, Shandong University, Jinan, 250100, China. ²National Key Laboratory of Application Specific Integrated Circuit (ASIC), Hebei Semiconductor Research Institute, Shijiazhuang, 050051, China. ³School of Mathematics, Shandong University, Jinan, 250100, China. ⁴Key Laboratory of Pulsed Power, Institute of Fluid Physics, CAEP, Mianyang, 621999, China. ⁵Microsystem and Terahertz Research Center, China Academy of Engineering Physics, Chengdu, 610200, China. Correspondence and requests for materials should be addressed to Z.L. (email: linzj@sdu.edu.cn)

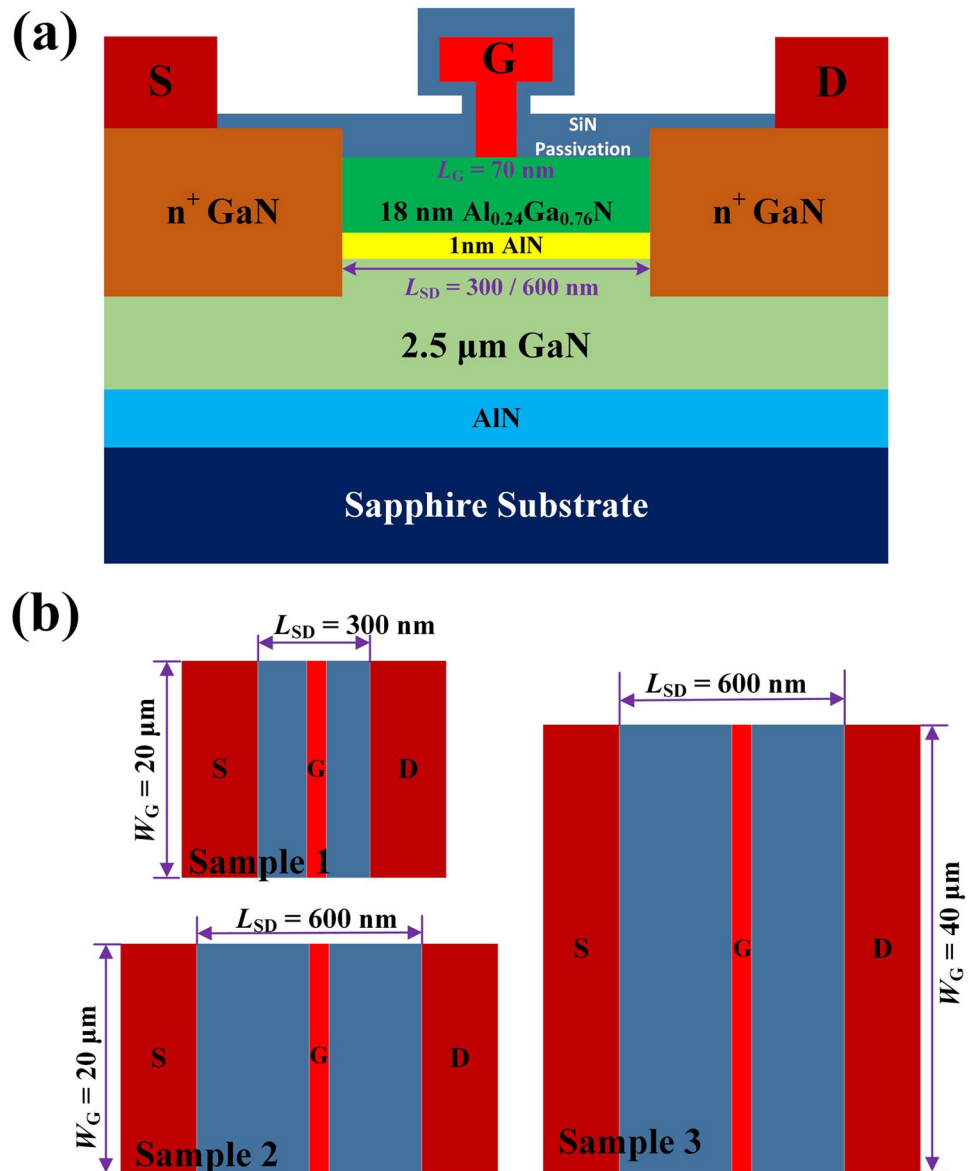


Figure 1. (a) Schematic of the AlGaN/GaN HEMTs. (b) Top views of the three samples.

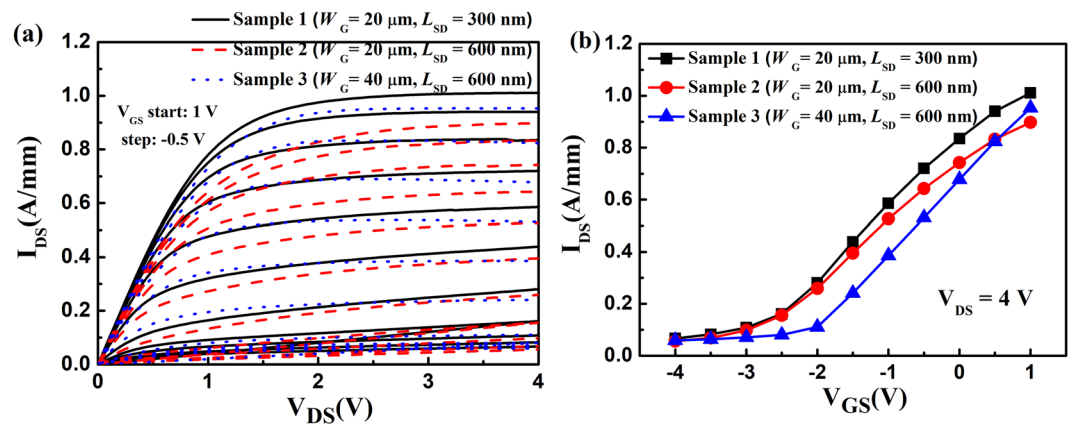


Figure 2. The measured (a) I - V out characteristics and (b) transfer characteristics (at drain-source voltage $V_{DS} = 4$ V) of the three samples.

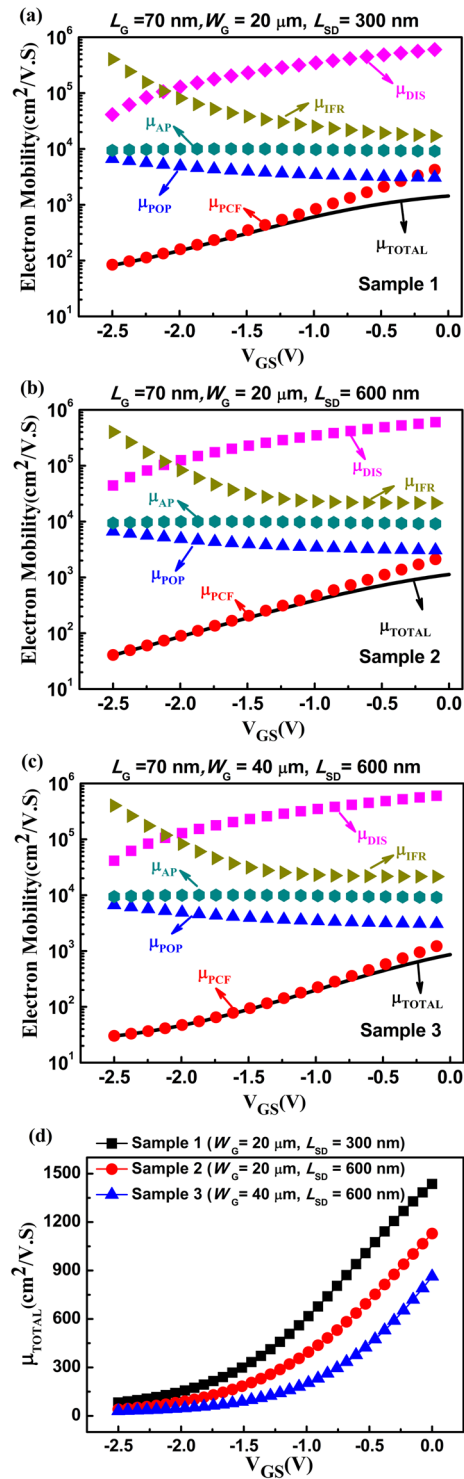


Figure 3. The detailed electron mobility as determined by PCF (μ_{PCF}), POP (μ_{POP}), IFR (μ_{IFR}), AP (μ_{AP}), and DIS (μ_{DIS}) scatterings, and the total electron mobility (μ_{TOTAL}) as a function of the gate-source voltage for (a) Sample 1, (b) Sample 2, and (c) Sample 3, respectively. (d) The total electron mobility (μ_{TOTAL}) versus the gate-source voltage for the three samples.

voltage V_{DS} of 100 mV at different gate biases were used. The main scattering mechanisms in the AlGaIn/GaN HEMTs include polar optical phonon (POP), polarization Coulomb field (PCF), interface roughness (IFR), acoustic phonon (AP), and dislocation (DIS) scatterings^{25,28,31,36–41}. Based on the two-dimensional scattering theory, the 2DEG electron mobility was obtained by applying the self-consistent iteration calculation^{25,26,42}, as shown in Fig. 3. The detailed parameters and calculation process are the same as in ref.⁴². As the gate-source voltage was decreased from 0 V to −2.5 V, the 2DEG electron mobility of the three samples decreased. The detailed electron

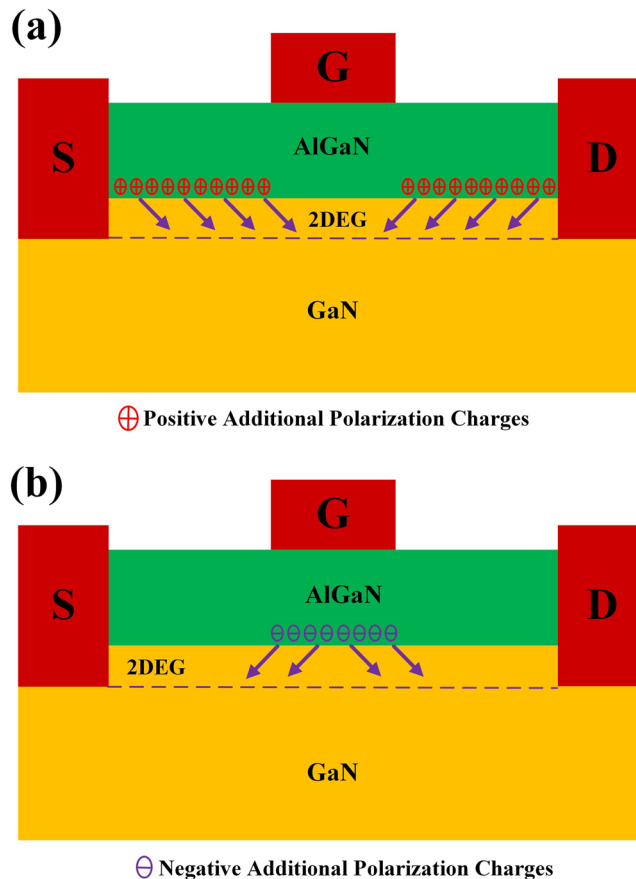


Figure 4. Schematic of the influence of the additional polarization charges on the 2DEG electrons (a) under the gate region and (b) under the gate-source/gate-drain region.

mobility determined by POP, IFR, AP, and DIS scatterings (labeled as μ_{POP} , μ_{IFR} , μ_{AP} , and μ_{DIS} , respectively) was the same for the three samples^{25,26}. However, the electron mobility determined by PCF scattering, labeled as μ_{PCF} , differed among the three samples. The PCF scattering in the 70-nm gate AlGaN/GaN HEMTs was the strongest scattering mechanism and obviously dominated the total electron mobility variation, causing the electron mobility to decrease with the gate bias. The electron mobility of Sample 2 was lower than that of Sample 1 but higher than that of Sample 3. This means that an increase in the source-drain distance or gate width can decrease the electron mobility.

Before the device processing, the strain distribution in the AlGaN barrier layer was consistent, and the polarization charges at the AlGaN/GaN interface were uniform^{21–24}. Because of the converse piezoelectric effect, the gate bias can change the strain of the AlGaN barrier layer under the gate region, causing the strain distribution of the AlGaN barrier layer to become nonuniform^{25–27}. The device scaling makes the nonuniformly distributed strain more obvious. This means that the non-uniform distribution of the polarization charges is enhanced. The PCF scattering, which originates from the nonuniform distribution of the polarization charges at the AlGaN/GaN interface, is also enhanced with the device scaling^{25,26,28,31–33}. The difference between the non-uniformly distributed polarization charges and the uniformly distributed ones is defined as the additional polarization charges. The negative gate bias decreases the tensile strain of the AlGaN barrier layer and reduces the polarization charges under the gate region^{25–27}. When the effect of the PCF scattering on the electron under the gate region is considered, as shown in Fig. 4(a), the positive additional polarization charges are located at the gate-source and gate-drain regions, which are increased with the decrease of the gate bias^{25–27}. The PCF scattering is enhanced by the increased additional polarization charges^{25–27,31–33}, causing the electron mobility to decrease with the decreased gate bias. Samples 1 and 2 have the same gate length and width. However, Sample 2 has bigger gate-source and gate-drain regions, as well as a larger number of additional polarization charges, compared with Sample 1. This means that the PCF scattering of Sample 2 is stronger than that of Sample 1. Therefore, Sample 2 has lower electron mobility. Samples 2 and 3 have the same gate length, gate-source spacing, and gate-drain spacing. Because Sample 3 has a bigger gate width, the increased additional polarization charges originating from this increased gate width enhances the PCF scattering^{34,35}; thus, Sample 3 has lower electron mobility than Sample 2.

Figure 5(a and c) shows the calculated parasitic access resistance versus the gate-source voltage. The gate-source parasitic access resistance (R_s) and the gate-drain parasitic access resistance (R_D) are obviously increased with the decreased gate-source bias. The difference between the parasitic access resistance under the negative gate bias (R_s and R_D) and that under the zero gate bias (R_{s0} and R_{D0}) was also obtained, as shown in

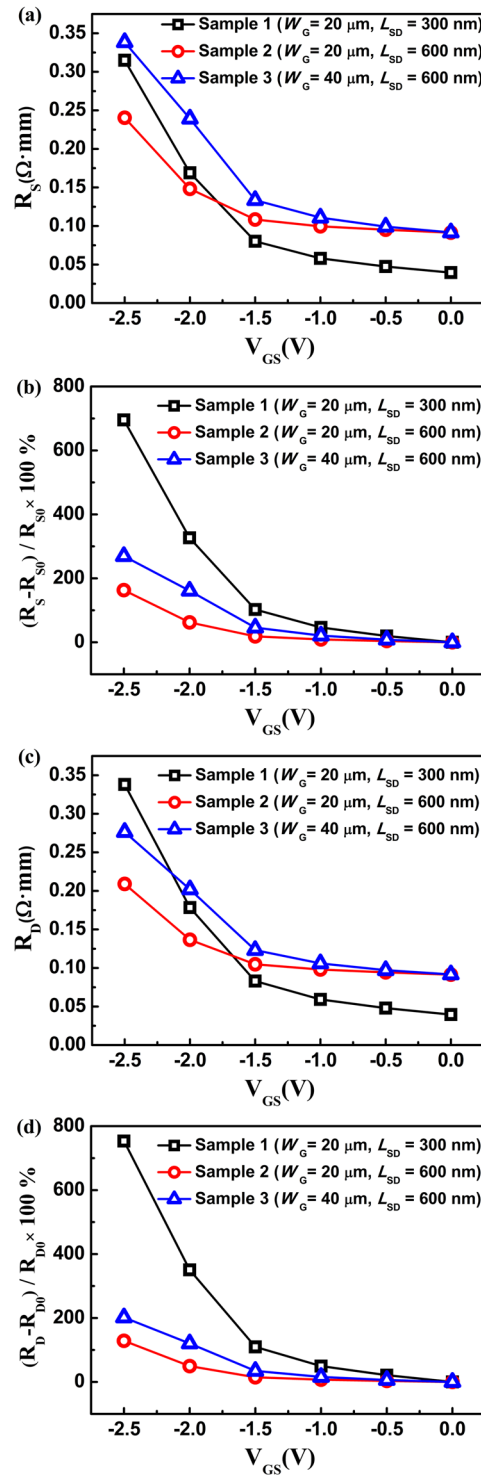


Figure 5. The obtained (a) source and (c) drain parasitic access resistance versus the gate-source voltage. The percentage variation of the (b) source and (d) drain parasitic access resistance corresponding to the source/drain access resistance at gate-source voltage $V_{GS} = 0$ V.

Fig. 5(b and d). Compared with the parasitic access resistance at gate-source voltage $V_{GS} = 0$ V, the parasitic access resistance at $V_{GS} = -2.5$ V showed an increase of approximately 700%. Furthermore, Samples 1 and 3 both showed a bigger increase than Sample 2. This means that the device with a smaller gate-source/gate-drain distance or a larger gate width has a more obvious increase in parasitic access resistance with the decreased gate-source bias.

Under the negative gate-source voltage, the polarization charges under the gate region are lower than those under the gate-source/gate-drain region. Therefore, considering the electrons in the gate-source/gate-drain channel, as shown in Fig. 4(b), the negative additional polarization charges were under the gate region, and increased

with the decreased gate-source bias^{24,25}. The increased additional polarization charges enhanced the PCF scattering and increased the parasitic access resistance. The additional polarization charges under the gate region are the same for Samples 1 and 2. However, Sample 1 has smaller gate-source/gate-drain distances than Sample 2. Thus, the influence of the additional polarization charges on the smaller gate-source/gate-drain distances is stronger^{24,25}, causing the PCF scattering to be enhanced and making the increase in the parasitic access resistances more obvious. Sample 3 has a bigger gate width, and the additional polarization charges under the gate region are larger for Sample 3 than for Sample 2. Furthermore, the PCF scattering is stronger and the parasitic access resistances showed a larger increase for Sample 3^{34,35}.

Conclusions

In summary, the electron mobility and parasitic access resistances versus the gate-source voltage for the 70-nm gate AlGaIn/GaN HEMTs were obtained. The PCF scattering, originating from the strain variation of the AlGaIn barrier layer, was shown to have a more significant influence on the device characterization with device scaling. This could present a possible approach toward improving the performance of 70-nm gate AlGaIn/GaN HEMTs by decreasing the PCF scattering.

Methods

Sample fabrication. The AlGaIn/GaN heterostructures were grown on a sapphire substrate by molecular beam epitaxy (MBE) (see Fig. 1(a) for a more detailed material structure description). The sheet electron concentration and electron mobility obtained from Hall measurements were $9.27 \times 10^{12} \text{ cm}^{-2}$ and $2020 \text{ cm}^2/\text{Vs}$, respectively. The AlGaIn barrier layer in the ohmic contact regions was etched into the GaN channel layer by inductively coupled plasma reactive ion etching (ICP-RIE), followed by MOCVD re-growth of highly Si doped n^+ -GaN ($3 \times 10^{19} \text{ cm}^{-3}$). The source and drain electrodes were formed by using non-alloyed Ti/Pt. The transmission-line matrix measurements showed that the ohmic contact resistance R_C was $0.58 \Omega \cdot \text{mm}$. Ni/Au T-shaped gate with a 70-nm gate length (L_G) was fabricated and located in the middle of the source and drain contacts. Finally, the devices were passivated by using 50-nm-thick SiN deposited by PECVD. As shown in Fig. 1(b), the device with $L_{SD} = 300 \text{ nm}$ and $W_G = 20 \mu\text{m}$ was labeled as Sample 1, the device with $L_{SD} = 600 \text{ nm}$ and $W_G = 20 \mu\text{m}$ as Sample 2, the device with $L_{SD} = 600 \text{ nm}$ and $W_G = 40 \mu\text{m}$ as Sample 3.

Measurements. The current-voltage (I - V) measurements were carried out at room temperature by using an Agilent B1500A semiconductor parameter analyzer.

References

- Brown, D. F., Tang, Y., Regan, D., Wong, J. & Micovic, M. Self-Aligned AlGaIn/GaN FinFETs. *IEEE Electron Device Lett.* **8**, 1445–1448 (2017).
- Zhou, H. *et al.* DC and RF Performance of AlGaIn/GaN/SiC MOSHEMTs With Deep Sub-Micron T-Gates and Atomic Layer Epitaxy MgCaO as Gate Dielectric Self-Aligned AlGaIn/GaN FinFETs. *IEEE Electron Device Lett.* **38**, 1409–1412 (2017).
- Huang, S. *et al.* Ultrathin-Barrier AlGaIn/GaN Heterostructure: A Recess-Free Technology for Manufacturing High-Performance GaN-on-Si Power Devices. *IEEE Trans. Electron Devices* **65**, 207–214 (2018).
- Chiu, H. C. *et al.* RF Performance of *In Situ* SiNx Gate Dielectric AlGaIn/GaN MISHEMT on 6-in Silicon-on-Insulator Substrate. *IEEE Trans. Electron Devices* **64**, 4065–4070 (2017).
- Zhang, K. *et al.* High-Linearity AlGaIn/GaN FinFETs for Microwave Power Applications. *IEEE Electron Device Lett.* **38**, 615–618 (2017).
- Vodapally, S. *et al.* Comparison for 1/f Noise Characteristics of AlGaIn/GaN FinFET and Planar MISHFET. *IEEE Electron Device Lett.* **64**, 3634–3638 (2017).
- Shinohara, K. *et al.* Scaling of GaN HEMTs and Schottky Diodes for Submillimeter-Wave MMIC Applications. *IEEE Trans. Electron Devices* **60**, 2982–2996 (2013).
- Chung, J. W. *et al.* AlGaIn/GaN HEMT With 300-GHz f_{max} . *IEEE Electron Device Lett.* **31**, 195–197 (2010).
- Bouazid-Driad, S. *et al.* AlGaIn/GaN HEMTs on Silicon Substrate with 206-GHz F_{MAX} . *IEEE Electron Device Lett.* **34**, 36–38 (2013).
- Shinohara, K. *et al.* Deeply-Scaled Self-Aligned-Gate GaN DH-HEMTs with Ultrahigh Cutoff Frequency. *Electron Devices Meeting (IEDM), 2011 IEEE Int.* 19.1.1–19.1.4 (IEEE, 5–7 Dec., Washington, 2011).
- Shinohara, K. *et al.* Self-Aligned-Gate GaN-HEMTs with Heavily-Doped n^+ -GaN Ohmic Contacts to 2DEG. *Electron Devices Meeting (IEDM), 2012 IEEE Int.* 27.2.1–27.2.4 (IEEE, 10–13 Dec., San Francisco, 2012).
- Nidhi. *et al.* N-polar GaN-based highly scaled self-aligned MIS-HEMTs with state-of-the-art ft-LG product of 16.8 GHz- μm . *Electron Devices Meeting (IEDM), 2009 IEEE Int.* 20.5.1–20.5.3 (IEEE, 7–9 Dec., Baltimore, 2009).
- Milosavljevic, I. *et al.* Vertically scaled GaN/AlN DH-HEMTs with regrown n^+ -GaN ohmic contacts by MBE. *68th Device Research Conference* 159–160 (2010). (21–23 Jun., South Bend, 2010).
- Guo, J. *et al.* MBE-Regrown Ohmics in InAlN HEMTs With a Regrowth Interface Resistance of $0.05 \Omega \cdot \text{mm}$. *IEEE Electron Device Lett.* **33**, 525–527 (2012).
- Micovic, M. *et al.* GaN Double Heterojunction Field Effect Transistor For Microwave and Millimeterwave Power Applications. *Electron Devices Meeting (IEDM), 2004 IEEE Int.* 807–810 (IEEE, 13–15 Dec., San Francisco, 2004).
- Palacios, T. *et al.* AlGaIn/GaN High Electron Mobility Transistors With InGaIn Back-Barriers. *IEEE Electron Device Lett.* **27**, 13–15 (2006).
- Ly, Y., Song, X., Guo, H., Fang, Y. & Feng, Z. High-frequency AlGaIn/GaN HFETs with f_T/f_{max} of 149/263 GHz for D-band PA applications. *Electron. Lett.* **52**, 1340–1342 (2016).
- Christy, P. D., Katayama, Y., Wakejima, A. & Egawa, T. High f_T and f_{MAX} for 100 nm unpassivated rectangular gate AlGaIn/GaN HEMT on high resistive silicon (111) substrate. *Electron. Lett.* **51**, 1366–1368 (2015).
- Marti, D. *et al.* C. R. 150-GHz Cutoff Frequencies and 2-W/mm Output Power at 40 GHz in a Millimeter-Wave AlGaIn/GaN HEMT Technology on Silicon. *IEEE Electron Device Lett.* **33**, 1372–1374 (2012).
- Shinohara, K. *et al.* Electron Velocity Enhancement in Laterally Scaled GaN DH-HEMTs with f_T of 260 GHz. *IEEE Electron Device Lett.* **32**, 1074–1076 (2011).
- Romanov, A. E., Baker, T. J., Nakamura, S. & Speck, J. S. Strain-induced polarization in wurtzite III-nitride semipolar layers. *Appl. Phys. Lett.* **100**, 023522 (2006).
- Bernardini, F. & Fiorentini, V. Spontaneous polarization and piezoelectric constants of III-V nitrides. *Phys. Rev. B* **56**, R10024–R10027 (1997).

23. Yu, E. T., Dang, X. Z., Asbeck, P. M., Lau, S. S. & Sullivan, G. J. Spontaneous and piezoelectric polarization effects in III–V nitride heterostructures. *J. Vac. Sci. Technol. B* **17**, 1742–1749 (1999).
24. Heikman, S. *et al.* Polarization effects in AlGaIn/GaN and GaN/AlGaIn/GaN heterostructures. *Appl. Phys. Lett.* **93**, 10114 (2003).
25. Cui, P. *et al.* Influence of Different Gate Biases and Gate Lengths on Parasitic Source Access Resistance in AlGaIn/GaN Heterostructure FETs. *IEEE Trans. Electron Devices* **64**, 1038–1044 (2017).
26. Yang, M. *et al.* Effect of Polarization Coulomb Field Scattering on Parasitic Source Access Resistance and Extrinsic Transconductance in AlGaIn/GaN Heterostructure FETs. *IEEE Trans. Electron Devices* **63**, 1471–1477 (2016).
27. Anwar, A. F. M., Webster, R. T. & Smith, K. V. Bias induced strain in AlGaIn/GaN heterojunction field effect transistors and its implications. *Appl. Phys. Lett.* **88**, 203510 (2006).
28. Zhao, J. *et al.* Electron mobility related to scattering caused by the strain variation of AlGaIn barrier layer in strained AlGaIn/GaN heterostructures. *Appl. Phys. Lett.* **91**, 173507 (2007).
29. Lv, Y. *et al.* Polarization Coulomb field scattering in AlGaIn/AlN/GaN heterostructure field-effect Transistors. *Appl. Phys. Lett.* **98**, 123512 (2011).
30. Luan, C. *et al.* Influence of the side-Ohmic contact processing on the polarization Coulomb field scattering in AlGaIn/AlN/GaN heterostructure field-effect transistors. *Appl. Phys. Lett.* **101**, 113501 (2012).
31. Luan, C. *et al.* Theoretical model of the polarization Coulomb field scattering in strained AlGaIn/AlN/GaN heterostructure field-effect transistors. *J. Appl. Phys.* **116**, 044507 (2014).
32. Yang, M. *et al.* Study of source access resistance at direct current quiescent points for AlGaIn/GaN heterostructure field-effect transistors. *J. Appl. Phys.* **119**, 224501 (2016).
33. Cui, P., Lv, Y., Lin, Z., Fu, C. & Liu, Y. Effect of polarization Coulomb field scattering on device linearity in AlGaIn/GaN heterostructure field-effect transistors. *J. Appl. Phys.* **122**, 124508 (2017).
34. Yang, M. *et al.* Study of Gate Width Influence on Extrinsic Transconductance in AlGaIn/GaN Heterostructure Field-Effect Transistors With Polarization Coulomb Field Scattering. *IEEE Trans. Electron Devices* **63**, 3908–3912 (2016).
35. Cui, P. *et al.* Improved Linearity with Polarization Coulomb Field Scattering in AlGaIn/GaN Heterostructure Field-Effect Transistors. *Sci. Rep.* **8**, 983 (2018).
36. Antoszewski, J. *et al.* Scattering mechanisms limiting two-dimensional electron gas mobility in $\text{Al}_{0.25}\text{Ga}_{0.75}\text{N}/\text{GaN}$ modulation-doped field-effect transistors. *Appl. Phys. Lett.* **87**, 3900 (2000).
37. Polyakov, V. M. *et al.* Intrinsically limited mobility of the two-dimensional electron gas in gated AlGaIn/GaN and AlGaIn/AlN/GaN heterostructures. *J. Appl. Phys.* **106**, 023715 (2009).
38. Gurusingham, M. N., Davidsson, S. K. & Andersson, T. G. Two-dimensional electron mobility limitation mechanisms in $\text{Al}_x\text{Ga}_{1-x}\text{N}/\text{GaN}$ heterostructures. *Phys. Rev. B* **72**, 045316 (2005).
39. Ridley, B. K., Foutz, B. E. & Eastman, L. F. Mobility of electrons in bulk GaN and $\text{Al}_x\text{Ga}_{1-x}\text{N}/\text{GaN}$ heterostructures. *Phys. Rev. B* **61**, 16862–16869 (2000).
40. Hsu, L. & Walukiewicz, W. Electron mobility in $\text{Al}_x\text{Ga}_{1-x}\text{N}/\text{GaN}$ heterostructures. *Phys. Rev. B* **56**, 1520–1528 (1997).
41. Oberhuber, R., Zandler, G. & Vogl, P. Mobility of two-dimensional electrons in AlGaIn/GaN modulation-doped field-effect transistors. *Appl. Phys. Lett.* **73**, 818 (1998).
42. Cui, P., Lin, Z., Fu, C., Liu, Y. & Lv, Y. A method to determine electron mobility of the twodimensional electron gas in AlGaIn/GaN heterostructure field-effect transistors. *Superlattices Microstruct.* **110**, 289–295 (2017).

Acknowledgements

This work was supported in part by the National Natural Science Foundation of China under Grant 11574182, Grant 11174182, Grant 61674130, Grant 11471194, Grant 11571115, and Grant 61504127, in part by the Developing Foundation of CAEP (key project) under Grant 2014A05011, and in part by the Science Challenge Project under Grant TZ2018003.

Author Contributions

P.C. and Z.L. contributed to the research design, experiment measurements, data analysis, and manuscript preparation. Y.L. fabricated the device. H.L. and A.C. carried out the mathematical calculation. C.F., C.L. and Y.Z. provided scientific advice. All authors critically edited the manuscript and approved the final version.

Additional Information

Competing Interests: The authors declare no competing interests.

Publisher's note: Springer Nature remains neutral with regard to jurisdictional claims in published maps and institutional affiliations.



Open Access This article is licensed under a Creative Commons Attribution 4.0 International License, which permits use, sharing, adaptation, distribution and reproduction in any medium or format, as long as you give appropriate credit to the original author(s) and the source, provide a link to the Creative Commons license, and indicate if changes were made. The images or other third party material in this article are included in the article's Creative Commons license, unless indicated otherwise in a credit line to the material. If material is not included in the article's Creative Commons license and your intended use is not permitted by statutory regulation or exceeds the permitted use, you will need to obtain permission directly from the copyright holder. To view a copy of this license, visit <http://creativecommons.org/licenses/by/4.0/>.

© The Author(s) 2018